Microporous and Mesoporous Materials 204 (2015) 218–225

Contents lists available at ScienceDirect

Microporous and Mesoporous Materials

journal homepage: www.elsevier.com/locate/micromeso

Propylsulfonic acid and methyl bifunctionalized TiSBA-15 silica as an efficient heterogeneous acid catalyst for esterification and transesterification

Camara Ibrahima Sory Léon [b], Daiyu Song [b], Fang Su [b], Sai An [b], Hongbo Liu [c], Jie Gao [c], Yihang Guo [a,*], Jiyan Leng [d,*]

[a] School of Environment, Northeast Normal University, Changchun 130117, PR China
[b] School of Chemistry, Northeast Normal University, Changchun 130024, PR China
[c] Changchun Institute of Optics, Fine Mechanics and Physics, Chinese Academy of Sciences, Changchun 130033, PR China
[d] First Hospital of Jilin University, Jilin University, Changchun 130021, PR China

ARTICLE INFO

Article history:
Received 30 May 2014
Received in revised form 13 November 2014
Accepted 19 November 2014
Available online 27 November 2014

Keywords:
Solid acid
Organosulfonic acid
Ordered mesoporous silica
Biodiesel
Inedible oily feedstocks

ABSTRACT

Propylsulfonic acid and methyl bifunctionalized TiSBA-15 silica material, TiSBA-15-Me-*Pr*SO_3H, is prepared by a direct nonionic surfactant-templated sol–gel co-condensation approach combined with low-temperature hydrothermal treatment. The structural integrity of the incorporated propylsulfonic acid groups and terminally bonding methyl groups are studied by ^{13}C CP-MAS NMR and ^{29}Si MAS NMR spectroscopy, while the chemical state of Ti(IV) species in the hybrid material is tested by XPS and UV–Vis/DRS. The ordered mesostructure, morphology and porosity of as-prepared hybrid material are characterized by low-angle XRD measurements, TEM observations and nitrogen gas porosimetry measurements. As the efficient solid acid catalyst, the heterogeneous acid catalytic activity and stability of the TiSBA-15-Me-*Pr*SO_3H are evaluated by esterification of palmitic acid and transesterification of yellow horn oil with methanol under refluxing temperature (65 °C) and atmospheric pressure. Based on the physicochemical properties and catalytic testing results, the excellent heterogeneous acid catalytic behaviors of as-prepared hybrid catalyst are explained by the contribution of their strong Brönsted and Lewis acidity, excellent porosity properties as well as surface hydrophobicity.

1. Introduction

Templated mesoporous silica materials, *e.g.* SBA, KIT and MCM series of inorganic silica and periodic mesoporous organosilica (PMO), possess excellent textural properties including large surface area, uniform pore-size distribution, high pore volume and tunable dimensionality of the pore channels and structural orderings; meanwhile, they also have abundant surface silanol groups that ensure them being easily functionalized by active sites. These unique properties lead to the functionalized mesoporous silica materials especial attractions in catalysis. Among various functionalized mesoporous silica materials, organosulfonic acid functionalized silica materials have been studied extensively. They are the robust solid acids possessing high Brönsted acid strength and plentiful number of acid sites. They have shown considerably high catalytic activity in a number of acid-catalyzed reactions including alkylation and acylation of hydrocarbons, hydration of alkenes, polymerization of THF, esterification, transesterification, hydrolysis and dehydration [1–4]. However, they often suffer from severe deactivation due to accumulation of organic or carbonaceous materials on the surface that blocks the acid sites; additionally, leaching of sulfonic acid group into the reaction media may also reduce the catalytic activity after several times' reaction cycles.

For the purpose of increasing total acidity and minimizing the adsorption of organic or carbonaceous materials on the surface of organosulfonic acid functionalized silica materials, herein, both titanium species and terminally bonding methyl groups are simultaneously incorporated to the framework of propylsulfonic acid-functionalized SBA-15 silica material through a direct sol–gel co-condensation method combined with low-temperature hydrothermal treatment. In the resulting TiSBA-15-Me-*Pr*SO_3H organic–inorganic hybrid material, the unsaturated surface Ti^{4+} species can provide Lewis acid sites, while the surface Ti−OH

* Corresponding authors. Tel./fax: +86 431 85098705.
E-mail address: guoyh@nenu.edu.cn (Y. Guo).

http://dx.doi.org/10.1016/j.micromeso.2014.11.018
1387-1811/

groups of TiSBA-15 framework can provide extra Brönsted acids sites except for protons from propylsulfonic acid groups. Additionally, surface hydrophobicity of SBA-15-*Pr*SO_3H can be enhanced due to the introduction of terminally bonding methyl groups. Both of the factors are beneficial in catalysis from the point of view of increasing acid catalytic activity and inhibiting deactivation of organosulfonic acid functionalized silica catalysts. The co-condensation route used in the present work is superior to the conventional surface grafting (post-synthesis) method because it can minimize processing steps and better control the loading and distribution of the functional groups as well as reinforce the interaction between the functionalities and SBA-15 silica support [5].

To evaluate the heterogeneous acid catalytic performance of as-prepared TiSBA-15-Me-*Pr*SO_3H organic–inorganic hybrid material, it has been applied in biodiesel production-related reactions under refluxing temperature (65 °C) and atmospheric pressure: esterification of palmitic acid (PA) and transesterification of yellow horn oil with methanol. Biodiesel is a mixture of C_{12}–C_{22} fatty acid monoalkyl esters (FAMEs), and it is a sustainable, sulfur-free, biodegradable and non-toxic fossil fuel substitute that is widely used worldwide [6,7]. Conventional catalysts for both of the reactions are homogeneous strong bases such as alkali metal hydroxides and alkoxides [8,9]. The base-catalyzed esterification and transesterification reactions can be carried out under mild conditions with high FAMEs yields. Unfortunately, homogeneous base catalysts suffer from drawbacks such as sensitivity to water and free fatty acids (FFAs, *e.g.* PA) that widely existed in low-cost oily feedstocks. Both of the components may induce saponification under alkaline conditions, which not only consumes the catalyst but also causes the formation of emulsions. Accordingly, virgin plant oils with FFA content less than 0.5%, an anhydrous alkali catalyst and anhydrous alcohol are necessary for commercially viable alkali-catalyzed production systems [10]. This requirement is a significant limitation to the use of low-cost feedstocks. As a result, biodiesel production by these routes is still not cost-competitive with petrodiesel. Biodiesel production processes based on the use of acid catalysts are good alternatives to conventional processes because of their simplicity and the simultaneous promotion of esterification and transesterification reactions from low-grade, highly-acidic and water-containing oils without soap formation. Highly reactive homogeneous Brönsted acid catalysts like HCl and H_2SO_4 are efficient for this process, but they suffer from serious contamination and corrosion problems that make essential the implementation of good separation and purification steps [11]. More recently, a "*green*" approach to biodiesel production has stimulated the application of sustainable solid acid catalysts (*e.g.* sulfated metal oxides, sulfonic ion-exchange resins, sulfonated carbon-based catalysts and acidic ionic liquids) as replacements for such liquid acid catalysts so that the use of harmful substances and generation of toxic wastes are avoided; meanwhile, the ease of catalyst separation after the reactions can be realized [12–14]. However, owing to low efficiency, most of solid acid-catalyzed esterification and transesterification processes proceed at higher temperature and higher pressure as well as higher methanol-to-oil molar ratio and longer reaction time. Therefore, the development of efficient solid acid catalysts for biodiesel production under mild conditions is still a challenge.

The catalytic activity of the TiSBA-15-Me-*Pr*SO_3H towards biodiesel production is also compared with Ti-free SBA-15-Me-*Pr*SO_3H, Ti- and methyl-free SBA-15-*Pr*SO_3H and commercially available sulfonic ion-exchange resin Amberlyst-15. Based on the catalytic testing results, contribution of Brönsted and lewis acidity, textural properties as well as surface hydrophobicity to the heterogeneous acid catalytic activity of as-prepared hybrid catalyst is revealed. Finally, the recyclability of the hybrid catalyst is tested through three consecutive catalytic runs.

2. Experimental

2.1. Materials

Tetraethoxysilane (TEOS), titanium isopropoxide (TTIP), 3-mercaptopropyltriethoxysilane (MPTMS) and Pluronic P123 (MW = 5800) were purchased from Aldrich and used without further purification. Methyltrimethoxysilane (MeTMS, 98%) was purchased from Alfa Aesar. Palmitic acid (99%) was purchased from Nankai University (Tianjin), China. Anhydrous methanol was obtained from Tianjin Guangfu Fine Chemical Research Institute, China. Yellow horn seed oil is commercially available.

2.2. Catalysts preparation

Pluronic P123 (4 g) was dissolved in a mixture of water (120 mL) and HCl (12 mol L^{-1}, 5.2 mL) at room temperature under vigorous stirring. The resulting homogeneous solution was heated to 40 °C, and then 7.8 mL of TEOS and 0.21 mL of TTIP were added, successively. After co-hydrolysis of TEOS and TTIP for 3 h, MPTMS (0.72 mL), MeTMS (0.55 mL) and hydrogen peroxide (1.1 mL) were added dropwise, respectively. The molar composition of the starting materials in the synthetic gel is P123:water:HCl:TEOS:TTIP:MPTMS:MeTMS:hydrogen peroxide = 0.02:191:1.78:1:0.02:0.1:0.1:0.34. The resulting mixture was continuously stirred at 40 °C for 24 h. The formed gel was subsequently transferred into a Teflon lined stainless autoclave and treated at 100 °C with a heating rate of 2 °C min^{-1} for 48 h. The resulting white solid powder was recovered by filtration, washed with deionized water and ethanol, and air-dried at room temperature overnight. P123 was removed from as-prepared material by washing with ethanol under reflux for 24 h (1 g per 50 mL ethanol). The process was repeated for four times to ensure most of P123 being removed. The solid was then recovered by filtration and dried in vacuum at 150 °C for 6 h. Ti loading in the TiSBA-15-Me-*Pr*SO_3H material is determined by ICP-AES, and it is 6.0 wt%.

2.3. Catalysts characterization

Low-angle XRD (LXRD) patterns were obtained on a D/max-2200 VPC diffractometer using Cu kα radiation. UV–Vis diffuse reflectance spectra (UV–Vis/DRS) were recorded on a Cary 500 UV–Vis–NIR spectrometer. FTIR spectra were recorded on a Nicolet Magna 560 IR spectrophotometer. TEM observations were performed on a JEM-2100F high resolution transmission electron microscope at an accelerating voltage of 200 kV. Nitrogen porosimetry measurement was performed on a Micromeritics ASAP 2020M Surface area and porosity analyzer after the samples were outgassed under vacuum at 363 K for 1 h and 373 K for 4 h. The surface areas were calculated using the Brunauer–Emmett–Teller (BET) equation, while pore size distribution curves were calculated using the Barrett–Joyner–Halenda (BJH) desorption branch of the isotherms, and the pore volume was accumulated up to $P/P_0 = 0.99$. ^{13}C CP-MAS NMR and ^{29}Si MAS NMR spectrums were recorded on a Bruker AVANCE III 400 WB spectrometer equipped with a 4 mm standard bore CP MAS probe head. The dried and finely powdered samples were packed in the ZrO_2 rotor closed with Ke–F cap which were spun at 12 kHz rate. Chemical shifts for ^{13}C CP-MAS NMR and ^{29}Si MAS NMR spectra were referenced to the signal of $C_{10}H_{16}$ standard ($\delta CH_2 = 38.5$) and 3-(trimethylsilyl)-1-propanesulfonic acid sodium salt standard ($\delta = 0.0$), respectively. XPS was performed on a VG-ADES 400 instrument with Mg Ka-ADES source at a residual gas pressure of below 10^{-8} Pa.

The types of acid sites (Brönsted and Lewis) of as-prepared hybrid material were distinguished by *in situ* FTIR spectroscopy

with chemical adsorption of pyridine. Catalyst sample was diluted with KBr and pre-treated at 100 °C for 12 h in vacuum. The sample was then exposed to pyridine vapor at 60 °C for 12 h in vacuum, followed by pumping out at 150 °C for 1 h to remove the physisorbed pyridine. Subsequently, FTIR spectrum of the pyridine-adsorbed sample was recorded.

2.4. Catalytic tests

The catalysts were dried for 2 h at 120 °C in a vacuum before the catalytic tests. All reactions were carried out in a three-necked round bottomed glass flask fitted with an alcohol cooled condenser. Esterification of palmitic acid with methanol was performed at 65 °C, palmitic acid to methanol molar ratio of 1:3 and 2 wt% (with respect to the amount of reactants) catalyst. Transesterification of yellow horn oil with methanol was performed at 65 °C, yellow horn oil: 1.1 mmol, methanol 99 mmol, 5 wt% (with respect to the amount of reactants) catalyst.

At periodical intervals, 0.1 mL of the reaction mixture was withdrawn and then diluted with acetone to 5 mL. The diluted suspension was centrifuged, and the clear solution was analyzed by a Shimadzu 2014C gas chromatograph (GC) to obtain the concentrations of the produced FAMEs. The GC was equipped with a HP-INNOWAX capillary column (film thickness, 0.5 μm; i.d., 0.32 mm; length, 30 m) and flame ionization detector. The operation temperature was 230 °C, flow rate of nitrogen gas was 1.0 mL min^{-1}, and ethyl laurate was applied as an internal standard. The catalytic activity of the catalysts was evaluated quantitatively by the yields of the FAMEs (Y, %). For the esterification of palmitic acid with methanol, Y was calculated as follows: $Y(\%) = (M_D/M_T) \times 100$, where M_D and M_T is the number of moles of methyl palmitate (MP) produced and expected, respectively. For the transesterification of yellow horn oil with methanol, Y was calculated as follows: $Y(\%) = (M_D/M_T) \times 100$, where M_D and M_T are the number of moles of FAMEs produced and expected, respectively.

2.5. Catalyst reusability test

To examine the catalytic stability of as-prepared TiSBA-15-Me-*Pr*SO_3H hybrid material in the transesterification process, the catalyst was tested at 65 °C. After the reaction, the catalyst was separated from the reaction mixture by centrifugation, washed three times with dichloromethane. Then the catalyst was separated and dried at 60 °C for subsequent catalytic run.

3. Results and discussion

3.1. Preparation and characterization of TiSBA-15-Me-PrSO$_3$H organic–inorganic hybrid catalysts

Titanium-containing SBA-15 silica material functionalized with both propylsulfonic acid groups and terminally bonding methyl groups (TiSBA-15-Me-*Pr*SO_3H) is successfully prepared by one-pot P123-assisted sol–gel co-condensation−hydrothermal treatment route, and the process includes the following steps. At first, co-hydrolysis of TEOS and TTIP in the presence of P123 for 3 h under strong acidity (pH < 1) is carried out to construct titanium-containing SBA-15 silica framework *via* Ti–O–Si linkage; meanwhile, nonionic surfactant P123 ($EO_{20}PO_{70}EO_{20}$, EO = ethylene oxide, PO = propylene oxide) is capable of self-assembling into a lyotropic liquid-crystalline phase at the beginning of stirring the $EO_{20}PO_{70}EO_{20}$ and inorganic precursors in an aqueous medium. This lyotropic liquid-crystalline phase can interact with the incomplete hydrolysis products of inorganic precursors through hydrogen bonding, which is the prerequisite to create ordered mesoporous titanium-containing silica materials. Subsequently, terminal-silylated organic precursor (*i.e.* MeTMS) and propylsulfonic acid precursor (*i.e.* MPTMS) are successively added in the above system to functionalize the above titanium/silica framework. The resulting mixture is continuously stirred at 40 °C for 24 h, and the formed gel suffers from low-temperature (100 °C) hydrothermal treatment for 48 h. After the above steps, methyl groups, coming from the hydrolysis of MeTMS, are terminally bonded on the titanium/silica framework *via* Ti–O–Si–C linkage; meanwhile, propylsulfonic acid groups, formed after the hydrolysis of MPTMS followed by *in situ* H_2O_2 oxidation, are incorporated into the titanium/silica framework *via* Ti–O–Si–C–S linkage. Finally, after boiling ethanol washing, P123 is removed from the hybrid material almost and then the mesostructured TiSBA-15-Me-*Pr*SO_3H hybrid materials are created. It should be noted that in order to avoid the decomposition of organofunctionalities (*e.g.* methyl groups and propylsulfonic acid groups), the removal of P123 by calcination should be avoided.

Based on the above preparation process, the wall structure of the TiSBA-15-Me-*Pr*SO_3H organic–inorganic hybrid material is proposed and presented in Scheme 1. The physicochemical properties of as-prepared TiSBA-15-Me-*Pr*SO_3H are characterized below.

3.1.1. Structural information

The structural integrity of the incorporated propylsulfonic acid groups and terminally bonding methyl groups in the TiSBA-15-Me-*Pr*SO_3H hybrid material are provided by solid state ^{13}C CP-MAS and NMR ^{29}Si MAS NMR spectra. Fig. 1a shows ^{13}C CP-MAS spectrum of TiSBA-15-Me-*Pr*SO_3H. Three distinct resonances at 11, 18, and 54 ppm correspond to C^1–C^3 carbon atoms on the propylsulfonic acid groups, *i.e.* H_3C^4–Si–O–Si–$C^3H_2C^2H_2C^1H_2$–SO_3H [15]. The result confirms the successful incorporation of propylsulfonic acid groups in the TiSBA-15 framework. Other resonance at −4 ppm is assigned to methyl carbon atoms attached to silicon (C^4) [16], suggesting that methyl groups are incorporated as a part of the framework of the hybrid materials. As for the rest of the unidentified resonance signals, they may be due to the residual surfactant, which is hardly to be removed completely even after hot ethanol washing for four times [17,18].

Fig. 1b shows ^{29}Si MAS NMR spectrum of TiSBA-15-Me-*Pr*SO_3H. Three resonances at −93, −102 and −111 ppm correspond to the siloxane species of $Si(OSi)_2(OH)_2$ (Q^2 band), $Si(OSi)_3(OH)$ (Q^3 band) and $Si(OSi)_4$ (Q^4 band), respectively, originating from the hydrolysis of inorganic silica precursor (*i.e.* TEOS) [19]. The other resonance at −67 ppm corresponds to the organosiloxane species of CH_3–$Si(OSi)_3$ (T^3 band), coming from the hydrolysis of organic silica precursor (*i.e.* MeTMS) [20]. The result further confirms methyl groups are incorporated into the TiSBA-15 silica framework.

The chemical state of the incorporated titanium species in the TiSBA-15-Me-*Pr*SO_3H hybrid material is studied by XPS analysis. From the result of high-resolution XP spectrum of TiSBA-15-Me-*Pr*SO_3H in the Ti $2p_{3/2}$ and Ti $2p_{1/2}$ binding energy regions shown in Fig. 2a it can obtain the binding energies of Ti $2p_{3/2}$ and Ti $2p_{1/2}$, and they are 458.9 and 464.8 eV, respectively. Compared with the binding energies of Ti $2p_{3/2}$ (458.7 eV) and Ti $2p_{1/2}$ (464.5 eV) in bulk TiO_2 that corresponds to Ti (IV) species of Ti–O–Ti [21], a slightly increased binding energies of Ti $2p_{3/2}$ and Ti $2p_{1/2}$ in as-prepared TiSBA-15-Me-*Pr*SO_3H hybrid material is inferred to the formation of part of Ti−O−Si linkage in the hybrid material.

UV–Vis diffuse reflectance spectroscopy is subsequently applied to further confirm the incorporation of Ti species in silicate network. Fig. 2b shows the normalized UV–Vis/DRS of as-prepared SBA-15-Me-*Pr*SO_3H and TiSBA-15-Me-*Pr*SO_3H. Compared with SBA-15-Me-*Pr*SO_3H material that shows poor absorption in the UV region, TiSBA-15-Me-*Pr*SO_3H exhibits obvious absorption band

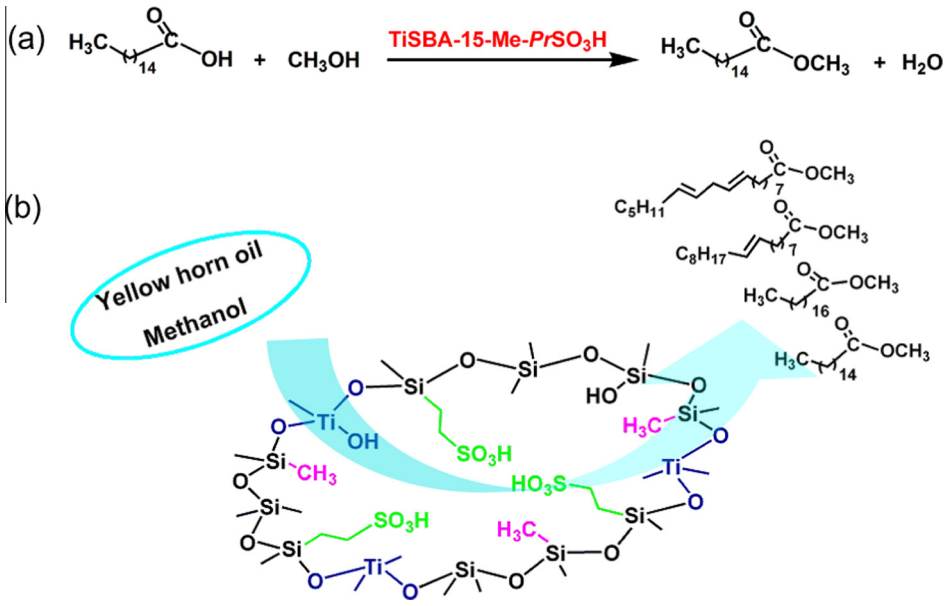

Scheme 1. Schematic presentation of wall structure of ordered mesoporous titanium-containing SBA-15 silica material functionalized with both propylsulfonic acid groups and terminally bonding methyl groups (TiSBA-15-Me-*Pr*SO_3H) (a) and the process of palmitic acid esterification and yellow horn oil transesterification over the TiSBA-15-Me-*Pr*SO_3H material (b).

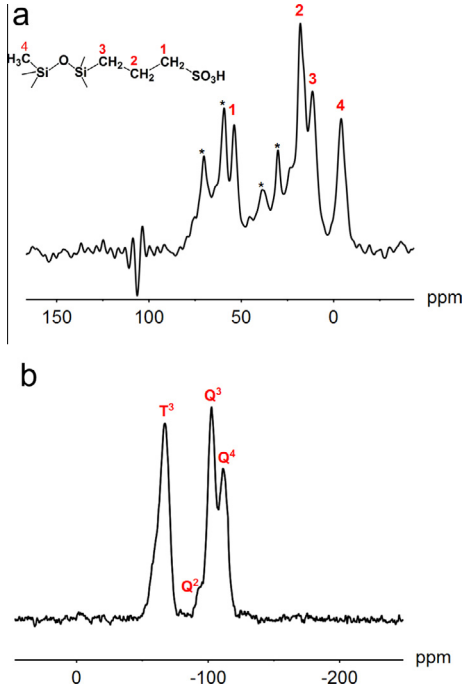

Fig. 1. ^{13}C CP-MAS NMR (a) and ^{29}Si MAS NMR (b) spectra of TiSBA-15-Me-*Pr*SO_3H material. The peaks labeled by asterisks indicate unidentified resonances.

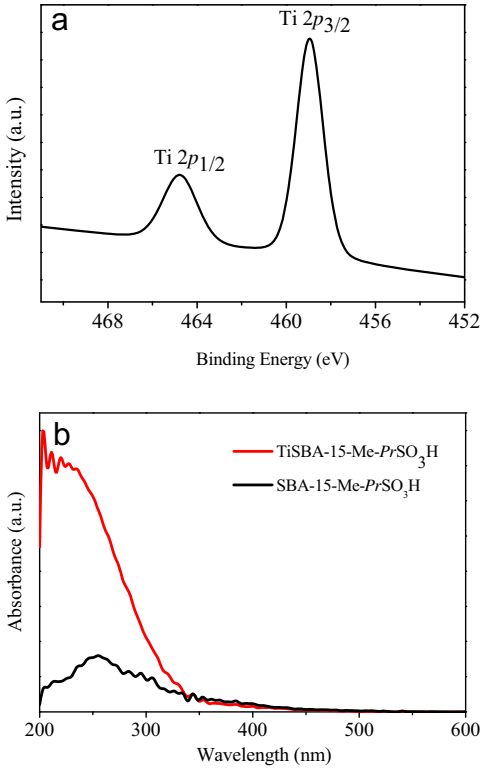

Fig. 2. High resolution XPS of TiSBA-15-Me-*Pr*SO_3H material in the Ti 3*d* binding energy region (a); the normalized UV–Vis/DRS of SBA-15-Me-*Pr*SO_3H and TiSBA-15-Me-*Pr*SO_3H (b).

in the range of 200–230 nm, which is originated from ligand-to-metal charge-transfer transition of isolated [TiO_4] or [$HOTiO_3$] units [22]. The result implies that at Ti content of 6 wt%, most of the titanium ions are incorporated and homogeneously distributed into the silicate frameworks.

3.1.2. Mesostructure, morphology and porosity

Mesostructure, morphology and porosity of TiSBA-15-Me-*Pr*SO_3H hybrid material are characterized by low-angle XRD measurements (Fig. 3), TEM observations (Fig. 4) and nitrogen gas porosimetry measurements (Fig. 5).

Fig. 3 displays the low-angle XRD patterns of various propylsulfonic acid-functionalized SBA-15 silica materials (*i.e.* SBA-15-*Pr*SO_3H, SBA-15-Me-*Pr*SO_3H and TiSBA-15-Me-*Pr*SO_3H). For comparison, the low-angle XRD pattern of SBA-15 silica is also provided. It shows that all tested samples exhibit three well-resolved peaks at 0.79 (intense), 1.37 (weak) and 1.60 (weak) deg, which are respectively indexed as the (100), (110) and (200) reflections of

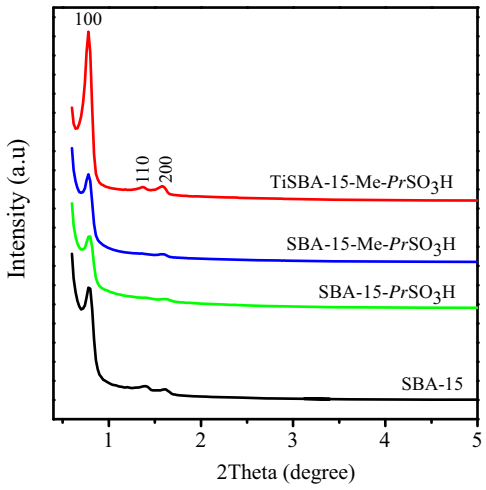

Fig. 3. Low-angle XRD patterns of various propylsulfonic acid-functionalized SBA-15 silica materials. For comparison, low-angle XRD pattern of SBA-15 silica is also presented.

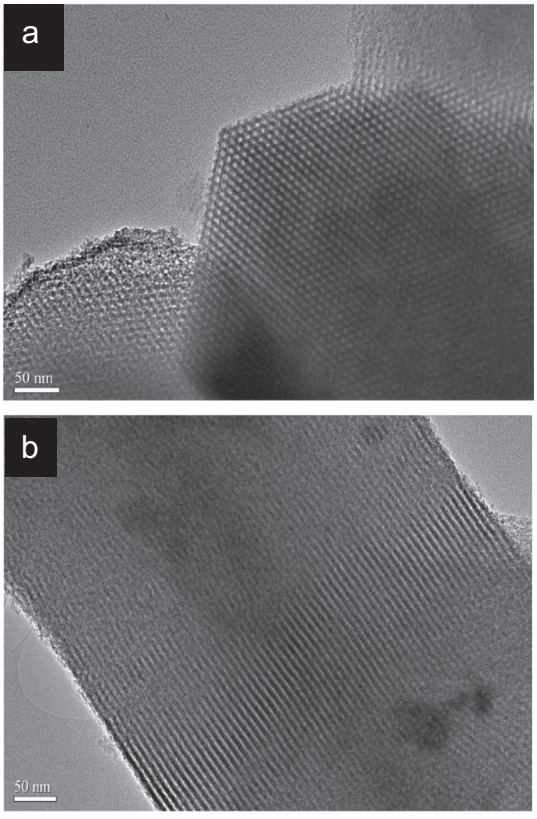

Fig. 4. TEM images of TiSBA-15-Me-PrSO$_3$H material recorded along (a) and perpendicular (b) to the channels axis.

p6mm hexagonal symmetry. The results indicate that the characteristic mesostructure of SBA-15 silica is retained after the incorporation of titanium, methyl groups and propylsulfonic acid groups into the silica framework.

The TEM observations (Fig. 4) support the above LXRD results, providing direct evidence for the highly ordered mesostructure of the TiSBA-15-Me-PrSO$_3$H hybrid material. The images show the material is 2D hexagonal mesostructures along the channel systems (Fig. 4a) and parallel stripes if viewed perpendicular to the channel directions (Fig. 4b).

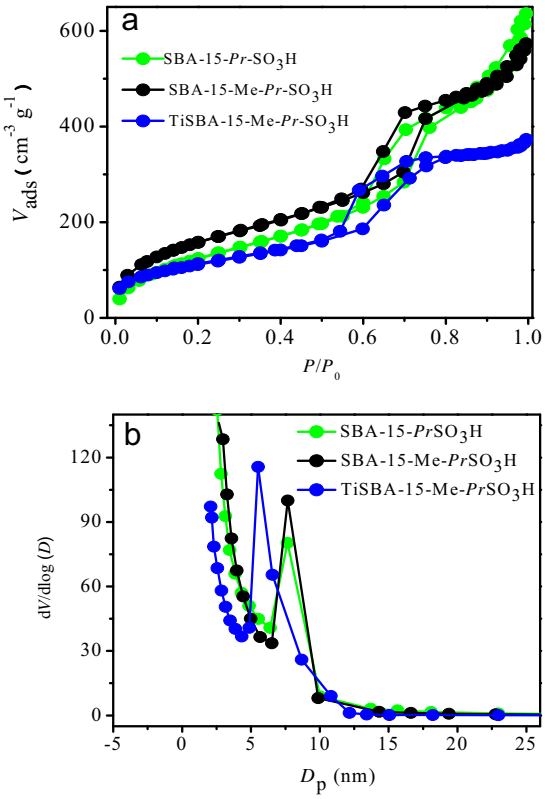

Fig. 5. Nitrogen adsorption–desorption isotherms (a) and pore size distribution curves (b) of various propylsulfonic acid-functionalized SBA-15 silica materials.

The overall mesoporosity of as-prepared various propylsulfonic acid-functionalized SBA-15 silica materials (*i.e.* SBA-15-PrSO$_3$H, SBA-15-Me-PrSO$_3$H and TiSBA-15-Me-PrSO$_3$H) is examined by nitrogen gas porosimetry, and the obtained adsorption–desorption isotherms and BJH pore-size distribution curves are shown in Fig. 5; meanwhile, the corresponding textural parameters are calculated and summarized in Table 1. From Fig. 5a it is found that three tested samples exhibit type IV isotherm with H1 hysteresis loop, characteristic of the materials with regular and even mesopores without interconnecting channels. Additionally, the sharp BJH pore-size distribution curve also indicates uniform pore diameters of the tested materials (Fig. 5b). The results are consistent with those of the LXRD and TEM. From Fig. 5a it is also observed that the onset of the capillary condensation step occurs at decreasing relative pressures for the SBA-15-PrSO$_3$H (P/P_0 = 0.60–0.80), SBA-15-Me-PrSO$_3$H (P/P_0 = 0.55–0.80) and TiSBA-15-Me-PrSO$_3$H (P/P_0 = 0.50–0.80). This implies that the pore diameter of propylsulfonic acid-functionalized SBA-15 silica materials decreases due to the introduction of methyl groups and/or Ti atoms to the silica

Table 1
Textural parameters and acid-site density of various propylsulfonic acid-functionalized SBA-15 silica materials.

Catalysts	S_{BET} (m^2 g^{-1})[a]	D_P (nm)[b]	V_P (cm^3 g^{-1})[c]
SBA-15-PrSO$_3$H	655	6.5	0.93
SBA-15-Me-PrSO$_3$H	660	5.7	0.85
TiSBA-15-Me-PrSO$_3$H	343	4.9	0.52

[a] Surface area (S_{BET}) was calculated using the Brunauer–Emmett–Teller (BET) equation.
[b] Pore diameter (D_p) was estimated from BJH desorption determination.
[c] Pore volume (V_p) was estimated from the pore volume determination using the adsorption branch of the nitrogen gas isotherms at P/P_0 = 0.99 single point.

framework. The conclusion is consistent with the pore diameter calculated from BJH desorption determinations, and the pore diameter of SBA-15-*Pr*SO_3H, SBA-15-Me-*Pr*SO_3H and TiSBA-15-Me-*Pr*SO_3H is 6.5, 5.7 and 4.9 nm, respectively (Table 1). From Table 1 it also can be seen that the BET surface area of TiSBA-15-Me-*Pr*SO_3H with Ti loading of 6.0 wt% decreases significantly (343 $m^2 g^{-1}$) compared with that of SBA-15-*Pr*SO_3H (655 $m^2 g^{-1}$) and SBA-15-Me-*Pr*SO_3H (660 $m^2 g^{-1}$). As for the pore volume of the tested samples, it decreases gradually for the SBA-15-*Pr*SO_3H, SBA-15-Me-*Pr*SO_3H and TiSBA-15-Me-*Pr*SO_3H.

3.1.3. Brönsted and Lewis acid properties

Pyridine adsorption-FTIR spectrum of TiSBA-15-Me-*Pr*SO_3H *is* provided to investigate the different types of acid sites in as-prepared hybrid material (Fig. 6). For comparison, FTIR spectra of SBA-15-Me-*Pr*SO_3H and pyridine-free TiSBA-15-Me-*Pr*SO_3H were also presented. Compared with FTIR spectra of SBA-15-Me-*Pr*SO_3H and TiSBA-15-Me-*Pr*SO_3H materials, three new characteristic peaks at 1450, 1490 and 1540 cm^{-1} are observed in the pyridine adsorption-FTIR spectrum of TiSBA-15-Me-*Pr*SO_3H. The peak at 1450 cm^{-1} is assigned to the Lewis acid sites, which is due to pyridine coordinatively bond to the unsaturated surface Ti^{4+}. As for the peak at 1540 cm^{-1}, it is related to pyridinium ions formed due to the protonation of the Brönsted acid sites. These Brönsted acids sites are contributed from the protons of propylsulfonic acid groups (predominant) and surface Ti–OH groups of TiSBA-15 framework (minor). The co-existence of Brönsted and Lewis acid sites is confirmed by the characteristic peak at 1490 cm^{-1}. The above results indicate that as-prepared hybrid material possess both Brönsted and Lewis acid sites.

3.2. Evaluation of heterogeneous acid catalytic performance of TiSBA-15-Me-*Pr*SO_3H organic–inorganic hybrid catalyst

3.2.1. Esterification of palmitic acid with methanol

The heterogeneous acid catalytic activity of as-prepared TiSBA-15-Me-*Pr*SO_3H organic–inorganic hybrid material is firstly evaluated by esterification of palmitic acid (PA) with methanol to yield methyl palmitate (MP) under the conditions of PA-to-methanol molar ratio of 1 to 3, 2 wt% catalyst, 65 °C and atmospheric pressure (Scheme 1a). For comparison, SBA-15-Me-*Pr*SO_3H, SBA-15-*Pr*SO_3H and SBA-15 silica are also tested under the same conditions. The esterification activity of the tested catalysts was represented by the yield of MP. From the result shown in Fig. 7 it is found that: (i) SBA-15 silica is inert to the target reaction, and formation of small amount of MP is due to the self-catalysis of PA; and (ii) for three tested propylsulfonic acid-functionalized SBA-15 silica materials, their catalytic activity follows the order SBA-15-*Pr*SO_3H < SBA-15-Me-*Pr*SO_3H < TiSBA-15-Me-*Pr*SO_3H. For example, the yield of MP reaches to 57 (SBA-15-*Pr*SO_3H), 74 (SBA-15-Me-*Pr*SO_3H) and 94% (TiSBA-15-Me-*Pr*SO_3H), respectively, after the reaction proceeded for 120 min.

3.2.2. Transesterification of yellow horn oil with methanol

To expand the scope of its application, the heterogeneous acid catalytic activity of as-prepared TiSBA-15-Me-*Pr*SO_3H hybrid material is further tested in transesterification of yellow horn oil with methanol to produce biodiesel under the conditions of methanol-to-oil molar ratio of 90 to 1, 5 wt% catalyst, 65 °C and atmospheric pressure. Low price and high yield of this inedible feedstock leads to the biodiesel-production process from inedible yellow horn oil is practical and economical. Thereby, biodiesel-derived from yellow horn oil is expected to be competitive with petroleum-based diesel for the commercial use.

In the TiSBA-15-Me-*Pr*SO_3H-catalyzed yellow horn oil transesterification system, the transesterification products (*i.e.* FAMEs) are identified by a GC–MS. The main FAMEs produced are methyl palmitate (MP, C16:0), methyl stearate (MS, C18:0), methyl oleate (MO, C18:1) and methyl linoleate (ML, C18:2); additionally, a small quantity of methyl eicosenoate (ME, C20:1) and methyl docosenate (MD, C22:0) are also found. Herein, the transesterification activity of the TiSBA-15-Me-*Pr*SO_3H is evaluated by the yields of four main FAMEs (*i.e.* MP, MS, MO and ML).

The transesterification activity of the TiSBA-15-Me-*Pr*SO_3H is firstly compared with commercially available reference catalyst, *i.e.* sulfonic ion-exchange resin Amberlyst-15. Amberlyst-15 possesses extremely high acid-site density [*i.e.* 4800 μeq(H^+) g^{-1}] [23], and it is widely used in transesterification reactions. From the result displayed in Fig. 8a it can be seen that the TiSBA-15-Me-*Pr*SO_3H shows significantly higher transesterification activity than that of Amberlyst-15. Over period of 9 h, the yields of MP, MS, MO and ML reach 62%, 71%, 62% and 37%, respectively, for TiSBA-15-Me-*Pr*SO_3H-catalyzed yellow horn oil transesterification reaction. Under the same conditions, the yields of MP, MS, MO and ML are 28%, 29%, 29% and 30%, respectively, for Amberlyst-15-catalyzed yellow horn oil transesterification reaction.

Fig. 8b presents the kinetics studies on TiSBA-15-Me-*Pr*SO_3H-catalyzed transesterification of yellow horn oil with methanol, and it is found that the transesterification reaction proceeds more slowly in comparison of esterification reaction. This result is explained by the following three reasons: (i) transesterification of triglycerides (TGs) in oily feedstocks is a more complex process

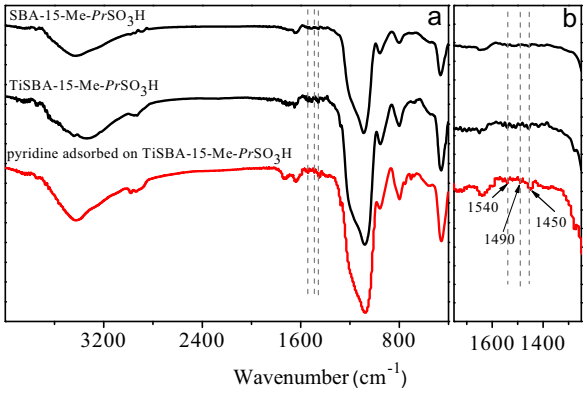

Fig. 6. FTIR spectra of SBA-15-Me-*Pr*SO_3H, pyridine-free TiSBA-15-Me-*Pr*SO_3H and pyridine-adsorbed TiSBA-15-Me-*Pr*SO_3H in the 4000–400 (a) and 1750–1250 cm^{-1} region (b).

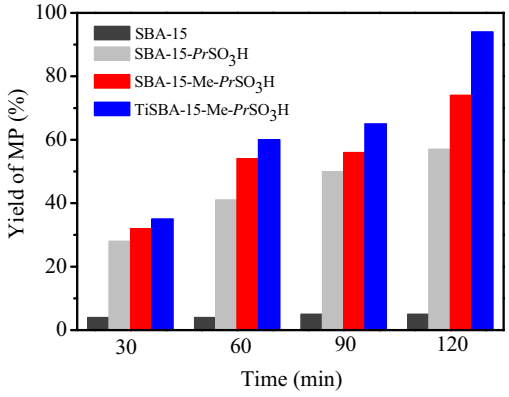

Fig. 7. Catalytic activity comparison of various propylsulfonic acid-functionalized SBA-15 silica materials in esterification of palmitic acid with methanol. Palmitic acid: 12 mmol, methanol: 36 mmol, catalyst 2 wt%, 65 °C, atmosphere refluxing.

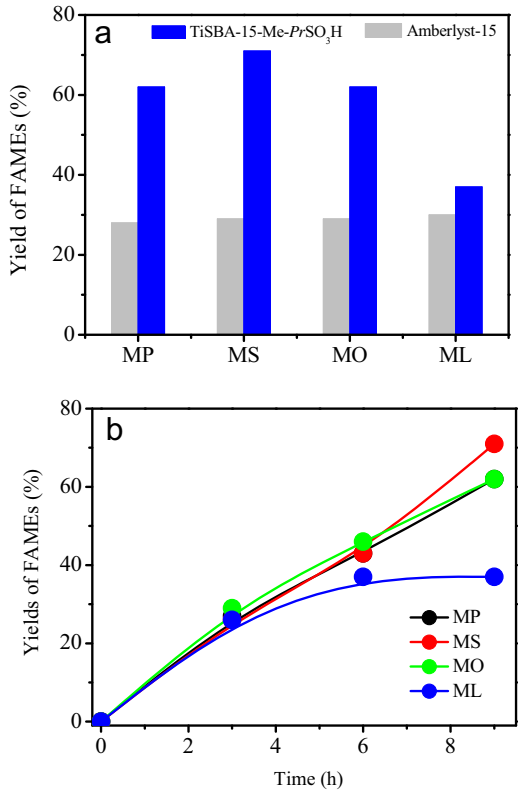

Fig. 8. Catalytic activity comparison of Amberlyst-15 and TiSBA-15-Me-*Pr*SO_3H towards transesterification of yellow horn oil with methanol (a); kinetics studies on TiSBA-15-Me-*Pr*SO_3H-catalyzed transesterification of yellow horn oil with methanol (b). Yellow horn oil: 1.1 mmol, methanol: 99 mmol, 5 wt% catalyst, 9 h, 65 °C, atmosphere refluxing.

with multiple steps; (ii) transesterification of TGs can produce more intermediates; and (iii) transesterification of TGs needs higher activation energy [12]. However, under mild conditions (*i.e.* 65 °C and atmospheric pressure), the transesterification activity of TiSBA-15-Me-*Pr*SO_3H is considerably high compared to many conventional solid acid catalysts [12].

3.2.3. Discussion

The above catalytic tests suggest that the heterogeneous acid catalytic activity of SBA-15-*Pr*SO_3H can be improved significantly after simultaneous incorporation of titanium species and terminally bonding methyl groups to its framework, which consequently permits the TiSBA-15-Me-*Pr*SO_3H-catalyzed palmitic acid esterification and yellow horn oil transesterification reactions perform at considerably fast rate under mild conditions. The excellent catalytic activity of TiSBA-15-Me-*Pr*SO_3H organic–inorganic hybrid catalyst is explained by the combination of enhanced total acidity contributed from both Brönsted and Lewis acid sites and the enhanced surface hydrophobicity due to the incorporated methyl groups. On the one hand, functionalization of SBA-15-*Pr*SO_3H by titanium species can also provide Lewis acid sites except Brönsted acid sites from *Pr*SO_3H group, which has been confirmed by pyridine adsorption-FTIR tests (Fig. 6). Both Brönsted and Lewis acid sites can facilitate the esterification and transesterification reaction. Firstly, the strong Brönsted acid property of the TiSBA-15-Me-*Pr*SO_3H hybrid catalyst plays a key role in its acid catalytic activity because the protonation of carbonyl groups of PA or TG molecules is the first and dominant step of the acid-catalyzed PA esterification or TG transesterification reaction. The strong Brönsted acidity of the hybrid catalyst can facilitate the reactions proceeding at fast rate. The Lewis acid sites of the hybrid catalyst come from coordinatively unsaturated Ti^{4+} sites of the TiSBA-15-Me-*Pr*SO_3H, which leave the exposed Ti^{4+} ion to interact directly with PA or TG molecules and act as the acceptor of the electron-pair. Accordingly, PA or TG molecules are activated. In the following steps, they follow the same procedures as those of the Brönsted acid-catalyzed esterification or transesterification reaction.

On the other hand, the enhanced surface hydrophobicity of the hybrid catalyst owing to incorporation of terminally bonding methyl groups in the framework is also responsible for the excellent esterification and transesterification catalytic activity. The hydrophobic environment in the pore channels is in favor of enrichment of hydrophobic reactants (*i.e.* PA or TGs), meanwhile, the hydrophilic byproducts (*i.e.* water or glycerol) are expelled. Accordingly, the accessibility of active sites to the reactants is increased, which can facilitate the esterification of PA and transesterification of yellow horn oil proceeding at fast rate. At the same time, the catalyst deactivation due to the strong interaction between the active sites and water or glycerol is dramatically reduced, which is confirmed by the following recycling test (Fig. 9).

Finally, it should be noted that although the BET surface area, pore diameter and pore volume of TiSBA-15-Me-*Pr*SO_3H decreased obviously compared with SBA-15-*Pr*SO_3H or SBA-15-Me-*Pr*SO_3H, it still possesses long-range ordered mesostructure with relatively large BET surface area and high pore volume. Accordingly, high population of the active sites can be provided for the esterification or transesterification reactions; meanwhile, ordered pore channels can decrease the mass transfer limit of the reactants and products. Both of the factors also can facilitate the reactions carried out at considerably fast rate.

3.2.4. Regeneration and reusability

One of the most important factors of heterogeneous catalysts contributing to catalytic performance is the stability against deactivation and leaching of the active sites during reaction. To evaluate this performance, recyclability of TiSBA-15-Me-*Pr*SO_3H in transesterification of yellow horn oil is tested through three consecutive catalytic runs. After the first catalytic run, the used catalyst is separated from the reaction mixture by centrifugation, and then it is washed with dichloromethane for three times. After being dried at 60 °C, the recovered catalyst is used for the second and third catalytic run, respectively, under the same experimental conditions and regeneration method. As shown in Fig. 9, the hybrid material showed a good catalytic stability maintaining a similar level of reactivity after three cycles. The result demonstrates that the sulfonic acid groups and methyl groups are strongly bonded to the TiSBA-15 silica framework and remain available as acid sites; meanwhile, catalyst deactivation due to the strong adsorption of hydrophilic byproducts is inhibited owing to the surface hydrophobicity of the hybrid catalyst.

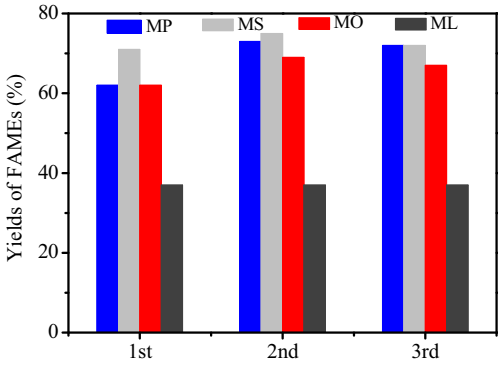

Fig. 9. Recyclability of TiSBA-15-Me-*Pr*SO_3H for the transesterification of yellow horn oil with methanol. Yellow horn oil: 1.1 mmol, methanol: 99 mmol, 5 wt% catalyst, 9 h, 65 °C, atmosphere refluxing.

4. Conclusions

Ordered mesoporous TiSBA-15-Me-*Pr*SO_3H organic–inorganic hybrid catalyst is successfully prepared through a direct P123-assisted sol–gel co-condensation–hydrothermal treatment route. By the combination of advantages including strong Brönsted and Lewis acidity, excellent porosity properties and hydrophobic surface, as-prepared TiSBA-15-Me-*Pr*SO_3H exhibits considerably high heterogeneous acid catalytic activity in esterification of palmitic acid and transesterification of yellow horn oil with methanol under mild conditions, and its catalytic activity outperforms commercially available sulfonic ion-exchange resin Amberlyst-15. Additionally, the hybrid catalyst can be reused at least three times without activity loss, attributing to the strong interaction between the functionalities (*i.e.* propylsulfonic acid groups and terminally bonding methyl groups) with TiSBA-15 silica framework as well as hydrophobic surface. Therefore, the hybrid catalyst exhibits potential as the efficient and stable solid acid catalysts in biodiesel production from low-cost inedible oily feedstocks.

Acknowledgement

This work was supported by the Natural Science Fund Council of China (21173036; 51278092).

References

[1] G.M. Ziarani, A.-R. Badiei, M. Azizi, Sci. Iranica 18 (2011) 453–457.
[2] T.M. Suzuki, T. Nakamura, E. Sudo, Y. Akimoto, K. Yano, Microporous Mesoporous Mater. 111 (2008) 350–358.
[3] M.H. Tucker, A.J. Crisci, B.N. Wigington, N. Phadke, R. Alamillo, J. Zhang, S.L. Scott, J.A. Dumesic, ACS Catal. 2 (2012) 1865–1876.
[4] J.A. Melero, L.F. Bautista, G. Morales, J. Iglesias, D. Briones, Energy Fuels 23 (2009) 539–547.
[5] I.K. Mbaraka, B.H. Shanks, J. Catal. 244 (2006) 78–85.
[6] R. Luque, J.C. Lovett, B. Datta, J. Clancy, J.M. Campelo, A.A. Romero, Energy Environ. Sci. 3 (2010) 1706–1721.
[7] K. Wilson, A.F. Lee, Sci. Technol. 2 (2012) 884–897.
[8] M.L. Granados, M.D. Zafra, Appl. Catal. B 73 (2007) 317–326.
[9] A.A. Kiss, A.C. Dimian, G. Rothenberg, Adv. Synth. Catal. 348 (2006) 75–81.
[10] Y. Wang, S. Ou, P. Liu, F. Xue, S. Tang, J. Mol. Catal. A 252 (2006) 107–112.
[11] S. Zheng, M. Kates, M.A. Dubé, D.D. McLean, Biomass Bioenergy 30 (2006) 267–272.
[12] F. Su, Y.H. Guo, Green Chem. 16 (2014) 2934–2957.
[13] C. Descorme, P. Gallezot, C. Geantet, C. George, ChemCatChem 4 (2012) 1897–1906.
[14] A. Sivasamy, K.Y. Cheah, P. Fornasiero, F. Kemausuor, S. Zinoviev, S. Miertus, ChemSusChem 2 (2009) 278–300.
[15] W. Li, K.J. Xu, L.L. Xu, J.L. Hu, F.Y. Ma, Y.H. Guo, Appl. Surf. Sci. 256 (2010) 3183–3190.
[16] K.J. Shea, G. Cerrato, S. Ardizzone, C.L. Bianchi, M. Signoretto, F. Pinna, Phys. Chem. Chem. Phys. 4 (2002) 3136–4507.
[17] W. Li, F.Y. Ma, F. Su, L. Ma, S.Q. Zhang, Y.H. Guo, ChemSusChem 4 (2011) 744–756.
[18] F. Su, L. Ma, D.Y. Song, X.H. Zhang, Y.H. Guo, Green Chem. 15 (2013) 885–890.
[19] Y. Sánchez-Vicente, C. Pando, M. Cortijo, A. Caba, Microporous Mesoporous Mater. 193 (2014) 145–153.
[20] A. Lúcia de Lima, A. Mbengue, R.A.S. San, Catal. Today 226 (2014) 210–216.
[21] F.Y. Ma, T. Shi, J. Gao, L. Chen, W. Guo, Y.H. Guo, S.T. Wang, Colloids Surf., A 401 (2012) 116–125.
[22] Z.L. Hua, W.B. Bu, Y.X. Lian, H.G. Chen, L. Li, L.X. Zhang, C. Li, J.L. Shi, J. Mater. Chem. 15 (2005) 661–665.
[23] Y.B. Huang, Y. Fu, Green Chem. 15 (2013) 1095.